



Original Article

Corrosion behavior of aluminum alloy in simulated nuclear accident environments regarding the chemical effects in GSI-191

Da Wang^{a, b, c}, Amanda Leong^b, Qiufeng Yang^b, Jinsuo Zhang^{b, *}^a Sino-French Institute of Nuclear Engineering and Technology, Sun Yat-Sen University, Guangdong, China^b Nuclear Material and Fuel Cycle Center, Department of Mechanical Engineering, Virginia Polytechnic Institute and State University, Blacksburg, VA, 24060, USA^c School of Nuclear Science and Engineering, North China Electric Power University, Beijing, 102206, China

ARTICLE INFO

Article history:

Received 2 September 2021

Received in revised form

30 May 2022

Accepted 29 June 2022

Available online 6 July 2022

Keywords:

LOCA

Corrosive coolant

Aluminum corrosion

Intermetallic

Passivation layer

ABSTRACT

Long-term aluminum (Al) corrosion tests were designed to investigate the condition that would generate severe Al corrosion and precipitation. Buffer agents of sodium tetraborate (NaTB), trisodium phosphate (TSP) and sodium hydroxide (NaOH) were adopted. The insulation materials, fiberglass and calcium silicate (Ca-sil), were examined to explore their effects on Al corrosion. The results show that significant precipitates were formed in both NaTB/TSP-buffered solutions at high pH. The precipitates formed in NaTB solution raise more concerns on chemical effects in GSI-191. A passivation layer formed on the surfaces of coupon in solution with the presence of insulations could effectively mitigate Al corrosion. The Fe-enriched intermetallic particles (IPs) embedded in coupon appeared to serve as seeds to readily induce precipitation via providing extra area for heterogeneous Al hydroxide precipitation. X-ray spectroscopy (EDS) and X-ray diffraction (XRD) analyses indicate that the precipitates are mainly boehmite (γ -AlOOH) and no direct evidence confirms the presence of sodium aluminum silicate or calcium phosphate.

© 2022 Korean Nuclear Society, Published by Elsevier Korea LLC. This is an open access article under the CC BY-NC-ND license (<http://creativecommons.org/licenses/by-nc-nd/4.0/>).

1. Introduction

During a loss of coolant accident (LOCA) in a pressurized water reactor (PWR), reactor coolant released at a highly energetic pipe break could dislodge materials nearby and generate debris [1]. The accumulation of debris on the sump strainers probably leads to flow resistance in the emergency core cooling system (ECCS). Thus, the United States Nuclear Regulatory Commission (USNRC) established the Generic Safety Issue (GSI)-191 [2]. The corrosion of materials in containment and the resulting corrosion products potentially contribute to the adverse impact on ECCS performance, which is called “chemical effects”. The Advisory Committee for Reactor Safety (ACRS) then raised concerns on sump performance issues related to chemical corrosion products [3]. A series of tests were conducted to verify whether the head loss across the sump strainer could be affected by chemical interactions between the exposed metals and recirculation water [4–7]. It is concluded that the gelatinous materials could form and transport to strainers,

causing an extra head-loss across the fibrous bed. The chemical effects on the flow resistance in fuel assembly were experimentally confirmed in recent studies [8,9]. These results lent credibility to the concerns issued by ACRS. Chemical products may also deposit on the fuel rods and impede decay heat removal, and precipitation-hard enable Al alloy progressively lose their ability to develop maximum strength and corrosion resistance [10,11].

A high boron concentration is present in the primary water to control reactivity and minimize volatilization of radioactive iodine. Several related studies reported that the high-temperature boric acid released from the reactor system was highly corrosive [12–15]. Furthermore, the containment spray system (CSS) may be injected with the solution at a high pH value. This fluid could corrode various metallic components in the containment building following a LOCA. The metallic ions were released into the cooling water, saturating the solution with soluble corrosion products, resulting in the formation of solid-phase precipitates. Even after the CSS stops, submerged surfaces of metallic components and physical debris would still contribute to corrosion or chemical reactions over a long period. Thus, the chemical products depend on the specific post-LOCA containment chemistry, involving the concentration of boric acid (H_3BO_3) and the buffering agents used to

* Corresponding author.
E-mail address: zjinsuo@vt.edu (J. Zhang).

neutralize the acidic coolant, such as trisodium phosphate (TSP), sodium tetraborate (NaTB) or sodium hydroxide (NaOH).

Some studies regarding GSI-191 focused on the potential impact of Al-containing precipitates on head-loss across the strainer [16–23]. These studies showed the significance of Al as a chemical effects source because Al components are often found in containment and have a propensity to release corrosion products, particularly in higher pH solutions. The pressure drop caused by Al precipitates was almost two orders of magnitude greater than that without chemical effects. So detailed investigation about the characteristics of Al corrosion and precipitation under specific chemical conditions is necessary. The Ca leaching from damaged fiberglass could also cause the generation of chemical precipitates. The main Ca releasing sources are the pipe insulation materials such as fiberglass and Cal-sil. The production of orthophosphates would dominate precipitation formation in Ca-containing carbonate systems when the concentration of phosphates was high enough [24]. The calcium orthophosphates generally are soluble in acids and less soluble in an alkaline solution. The type of calcium orthophosphate depends on the solution pH, temperature, and molar ratio of phosphorous (P) to Ca. However, the previous Ca-leaching tests were short and not conducted with the presence of TSP, resulting in insufficient information about Ca releasing from insulation in TSP-buffered solutions [25].

Although the factors that influence Al corrosion have been well explored, the factors affecting Al corrosion products release, which is more relative to strainer blockage, were not. The tests using TSP as buffering agent performed by the CHLE program [26] failed to produce enough Al corrosion to induce precipitate formation. Although lack of Al precipitates is a desirable outcome regarding GSI-191, such prototypical tests did not provide a basis for specific conditions that would lead to Al precipitation, nor the characteristics of the precipitates if formed. To obtain a reasonable estimation of the conditions, identity and quantify the formed precipitates, it is desirable to design non-prototypical tests with extreme conditions to force Al precipitation to occur.

2. Experiments and material

2.1. Experiment system

The primary components of the shaker table test system are a shaker equipped with a variable speed drive, a high-stability immersion digital circulator, and a rectangular polypropylene tank with the dimensions of $50 \times 50 \times 30$ cm, as shown in Fig. 1. The tank is placed on the tray of the shaker. One liter Nalgene polypropylene bottles loading test solution are set inside 5×5 ports of bottle holder supported by the tank. Each content designed on the bottle can represent an identical but separate experiment. Copper pipes were configured in a square “U” pattern across the tank bottom with specific separation distance. The water in the pipes is circulated and heated by an immersion digital circulator (built-in heater and temperature control unit). The temperature of

circulating water heater was set a few degrees above the target temperature for maintaining the solution temperature at aimed value. There is a total immersion thermometer in the water tank, when the test solution is heated to the desired temperature, the coupons are inserted into the bottles and suspended in a symmetric pattern (the central location of the solution) by nylon string. Place bottles back into the bottle holder and record the time. This will be the start time of the test duration. The solution and coupon were collected at the prescribed time. All shaker table tests were carried out at a constant speed of 75 revolutions per minute (rpm) to simulate the sump water conditions.

2.2. Test chemicals

The dry buffering agent is generally present in baskets on containment floor and starts to dissolve once exposed in post-LOCA recirculation water. Both TSP and NaTB are suitable buffers for placement in containment. If NaOH is included in the safety injection system, it will cause higher sump water pH and corrosion rate than other buffering agents. Precipitates were observed to form either fine or cloudy suspensions that presented a negligible tendency to settle in the slightly alkaline solution containing 2500 mg/L of boron [21]. Accordingly, a non-prototypical pH value is necessary to intensify chemical precipitation. Therefore, the test solutions have different pH values and buffer chemistry due to the varying chemical requirements. Once the predetermined amounts of chemicals were added for each test, no attempt was made to control or alter the resulting pH during the test.

Al alloy 1100 was adopted as the Al source in this study. All tests used an approximate metal surface area to solution volume ratio of $2.64 \text{ m}^2/\text{m}^3$ (the dimension of aluminum coupon sample is $25.4 \times 25.4 \times 1.6 \text{ mm}^3$, the volume of test solution was 0.55 L). Table 1 lists the elemental compositions of Alloy 1100. Fiberglass and Ca-sil used as insulation samples were exposed in testing solution to determine if any chemical compounds like calcium phosphate or sodium aluminum silicate are formed during test. The results from the bench top leaching tests [27] showed that the amount of Ca leached was independent on the extent of fiberglass destruction (clump and blended). Thus, the insulations were cut into pieces. Each patch of fiberglass and Ca-sil was secured in a stainless-steel mesh ball that allowed solution flow while confining the insulation materials.

The long-term Al precipitation tests program includes seven tests under different hypothesized conditions. The physical and chemical parameters defining the solution environments are summarized in Table 2. Three critical parameters were investigated in this study. The first variable is the buffer used to neutralize the sump water. The second variable is the pH, a target pH was achieved by adding NaOH. The third variable is the presence of insulation that might produce other precipitates. The Test 2 was performed twice because the coupons fell from the string into solution during the test.

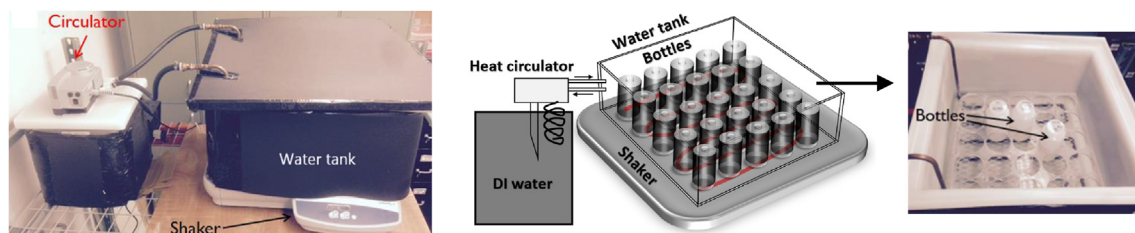


Fig. 1. Shaker table test system.

Table 1

Alloy 1100 elemental composition (wt %).

Elements	Fe	Si	Cu	Mn	Mg	Cr	Ni	Ga	Zn	Ti	V	Al
Concentration	0.41	0.1	0.06	0.009	0.006	0.002	0.007	0.01	0.004	0.01	0.024	Balance

Table 2Test conditions in test solution^a.

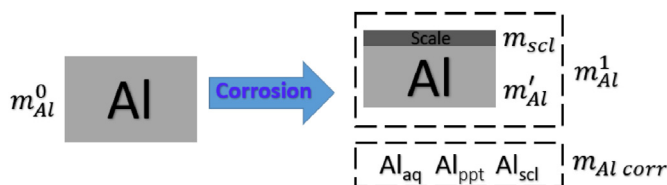
Test no.	Boron content (mg/L)	Buffer agent ^b	15 M NaOH (ml)	pH _{25°C}	Insulation (g/L)	
					Fiberglass	Ca-Sil
1	2550 ^c	TSP	1.8	8.5	-	-
2	2550	TSP	7.4	10.0	-	-
3	2550	TSP	7.4	10.0	1.0	1.0
4	2380 ^d	NaTB	1.5	8.2	-	-
5	2380	NaTB	5.0	9.5	-	-
6	2380	NaTB	7.0	10.0	-	-
7	2380	NaTB	7.0	10.0	1.0	1.0

^a Temperature was maintained at 85 °C in all tests.^b TSP: Na₃PO₄·12H₂O, NaTB: Na₂B₄O₇·10H₂O.^c The 2550 mg/L boron concentration was achieved by adding 14.6024 g/L of H₃BO₃ and 4.8172 g/L of TSP. For Test #4–7, the 2380 mg/L boron was added as 11.5067 g/L H₃BO₃ and 3.2683 g/L of NaTB.

2.3. Analytical methods

The aqueous samples were collected at the prescribed time for Al concentration measurement by Inductively Coupled Plasma Mass Spectrometry (ICP-MS) and precipitation observation. After immersion reached the specific duration, the coupons were retrieved, rinsed with DI water followed by ethanol, allowed to air dry and cool to room temperature, photographed and weighed. The coupons were then descaled according to procedures in ASTM G1-03 [28]. The cleaning method is designed to remove the bulky corrosion products on the coupon and avoid reactions that may result in excessive removal of base Al. After descaling, the coupons were rinsed, and weighed again after drying. The Al concentration data can represent the Al corrosion for a clear solution without visualized particles. When strong precipitation happens, the coupon weight change data can assess the Al corrosion. With reference to Fig. 2, the mass balance for corroding aluminum is given by Eq. (1), where m_{Al}^0 is the initial mass of the coupon; m'_{Al} is the mass of coupon after descaling; $m_{Al\ corr}$, the total corroded Al, is the sum of the mass of Al in the scale Al_{scl} , solution Al_{aq} and precipitates Al_{ppt} . The m'_{Al} can be calculated by Eq. (2), where m_{scl} is the mass of scale formed on coupon surface, m_{Al}^1 is the mass of coupon after test. After rearrangement, the $m_{Al\ corr}$ can be derived by Eq. (3). During the tests, m_{scl} was extremely small, around 6.2 % of $m_{Al\ corr}$. Thus, the difference between m_{Al}^0 and m_{Al}^1 , i.e. the mass loss of coupon before and after test is an indicator of the rate of Al corrosion.

$$m_{Al}^0 = m'_{Al} + m_{Al\ corr} \quad (1)$$

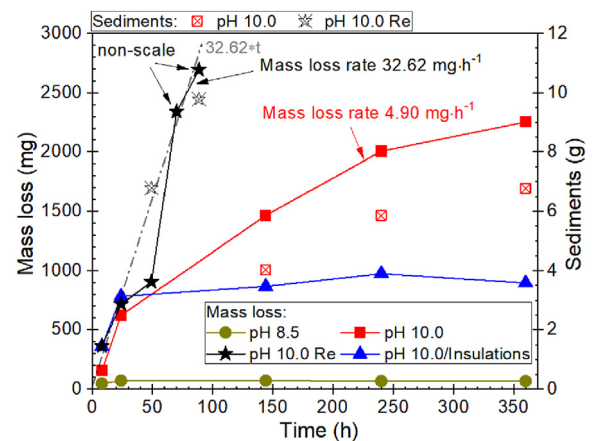
**Fig. 2.** Illustration of aluminum mass balance.

$$m'_{Al} = m_{Al}^1 - m_{scl} \quad (2)$$

$$m_{Al\ corr} = m_{Al}^0 - m_{Al}^1 + m_{scl} \quad (3)$$

$$\text{Mass loss (mg)} = m_{Al}^0 - m_{Al}^1 \quad (4)$$

A photograph tracking of coupon surface after exposure to test solution was performed. Some representative metal coupons and sediments were selected to visualize the morphology of the materials and evaluate the present chemical species by scanning electron microscopy (SEM) and energy dispersive X-ray spectroscopy (EDS) techniques. A brighter region in the back-scattered electron (BSE) mode can indicate presence of heavier elements. The visual inspection of the coupons, zoom-in image of the rectangular region and chemical composition were shown by the insets. X-ray diffraction (XRD) analyses were also carried out to confirm the sediment identity.

**Fig. 3.** Measured mass loss of coupon and sediments mass in TSP-buffered solution.

3. Experimental results

3.1. Solution with buffering TSP

A comparison of mass loss of coupons immersed in TSP-buffered solution was illustrated in Fig. 3. The results show remarkable corrosion in solution using high pH comparing with less alkaline solution.

When solution pH was 8.5 or there were insulations, the mass loss of coupons started to level off at 24 h. When pH was 10.0 and without insulation material, the coupons continuously lost weight until totally dissolved into solution. During the tests, the formed scales were visible through the change in appearance. When the coupons were not covered by scales, there is a linear dependence of mass loss with time and the mass-loss rate was apparently high, suggesting the significant effect of pH on Al corrosion. The data in the figure had been fitted using a simple kinetic equation of $[ML] = k \cdot t$. The coefficient k is the mass-loss rate. The k of coupon without scale approached 32.62 mg/h, almost seven times higher than that with scale (4.90 mg/h). The mass loss at 48 h (pentagram symbol) deviated from the fitting line (dot-dashed line) because a protective layer formed on the coupon.

The intense precipitation occurred in all solutions at pH 10.0, while no precipitates were observed at pH 8.5. The related analysis regarding precipitation will be presented in later sections. The sediment in the bottom of bottle was collected, dried and weighed. As shown in Fig. 3, the sediment mass increased stably with the coupon corrosion. More sediments were found in Test 2-Re because the coupon in Test 2 fell from string and was covered by sediments, the corrosion was thereby retarded partly. These results suggest that the TSP-buffered solution at pH 10.0 could cause severe Al corrosion and precipitation. The insulation could induce the formation of a passivation layer which impeded corrosion. The Al corrosion was insignificant in Chen's tests where Ca-sil was used as the primary insulation material in combination with fiberglass [15]. And the subsequent studies confirmed the inhibition of Al corrosion was by silicate [29,30].

Fig. 4 illustrates the surfaces of unused coupon and the coupon without forming scale after exposure in TSP solution. These coupons all present a shiny appearance. From the SEM images, the unused coupon has a relatively smooth surface, while a rough coupon surface with pits was observed after exposure. The clear polishing scratch on unused coupon surface, more-observed scratch on surface of coupon in solution with pH 8.5, and no scratch on surface of coupon in solution with pH 10.0 indicate the most severe corrosion at pH 10.0, it is confirmed by the amounts of the hemispherical shape of trenches on coupon surface. IPs were identified on coupon surfaces, which is more noticeable in the BSE images. Birbilis found the IPs range in size from angstroms to

10 μm , depending on the type of particles [31]. The major impurities in Al alloy 1100 are Fe and Si, and Al–Fe–Si ternary intermetallic compounds such as FeAl_3 , $\text{Fe}_3\text{SiAl}_{12}$, $\text{Fe}_3\text{Si}_2\text{Al}_9$, $\text{Fe}_2\text{Si}_2\text{Al}_9$, etc. [32]. Based on the EDS analyses, the Al alloy in this test has Fe-bearing IPs with a small fraction of Si and Cu, which appears to be consistent with previous literature data. Moreover, since the ICP-MS analyses for solution samples did not show any significant Fe concentration, it seems that Fe in the particles originated from the Al coupon itself. The local degradation resulted from galvanic interactions between the IPs and their adjacent alloy matrix [33,34]. A higher oxygen (O) peak was detected in Fe-enriched particles compared to the Al matrix, indicating that the surfaces of these particles are some oxides or covered by Al hydroxide precipitates. A possible reason is that the IPs serve as seeds for heterogeneous Al hydroxide precipitation, which is further discussed in the next section.

Several types of scale were observed during the tests. Fig. 5 compares the SEM images of scales formed in TSP-buffered solution at different pH and exposure time. The entire surface of the coupons in solution at pH 8.5 were uniformly corroded from 24 h to 360 h. The EDS analyses show that the scattered particles are Fe-bearing intermetallics (Fig. 5a). The ratio of O to Al in the black scale is 1.67, this scale could be Al_2O_3 . The appearance of sodium (Na) and phosphorus (P) on surfaces were possibly caused by TSP residue, or some portion of the scale consisted of aluminum phosphate (AlPO_4). The aluminum phosphate and aluminum oxide are white in color and crystalline in form under most conditions. Some oxides are blackened during formation under volatile conditions, so the elevated temperature and specific chemistry may blacken the aluminum oxide layer as it formed [35]. Fig. 5b–d shows the scale morphology formed in solution at pH 10.0. A darker surface was observed at 8 h. The population density of particulate on the coupon surface is higher than others. Physically, the dense particulates formed a crust-like substance on coupon surface. EDS analysis of these particles shows higher enrichment of Mn, which comes from Al 1100 alloy as the impurity. There is no significant IPs on the coupon surface at 48 h (Fig. 5c) and most surface area is coated by aluminum oxide. The coupon appears heavily damaged by corrosion after 144 h (Fig. 5d). The texture of the particulate on the scale is powdery (Fig. 5d) and presents the same chemical composition with the scale, suggesting that these corrosion products may form as particles and continuously grow as solid scale on surface. The ratio of O to Al from these corrosion products is 2.2–3.2, consistent with the composition of AlOOH and $\text{Al}(\text{OH})_3$.

Godard [36] suggested that the aluminum oxide formed was initially hydrated amorphous $\text{Al}(\text{OH})_3$, which dehydrated with time and transformed to bayerite ($\alpha\text{-Al}(\text{OH})_3$) and boehmite ($\gamma\text{-AlOOH}$), depending on temperature. Vargel [37] delineated the temperatures initiating these transitions were: amorphous aluminum oxide

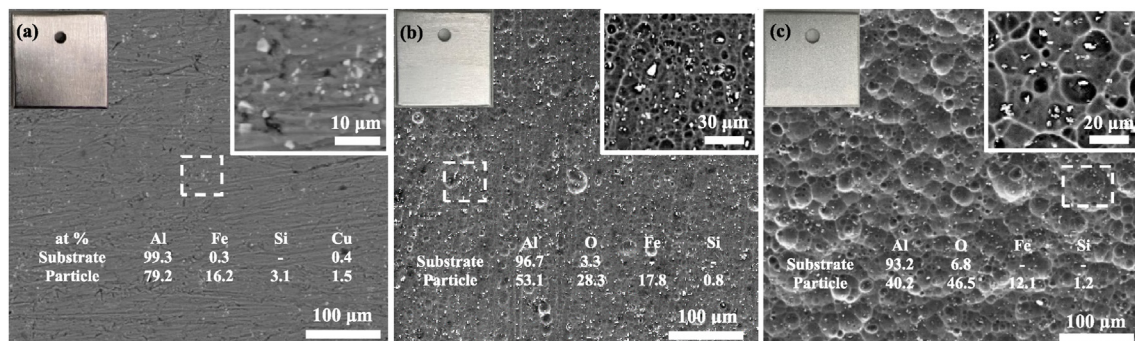


Fig. 4. SEM images of Al coupon of (a) unused; (b) TSP-pH 8.5 at 8 h; and (c) TSP-pH 10.0 at 24 h.

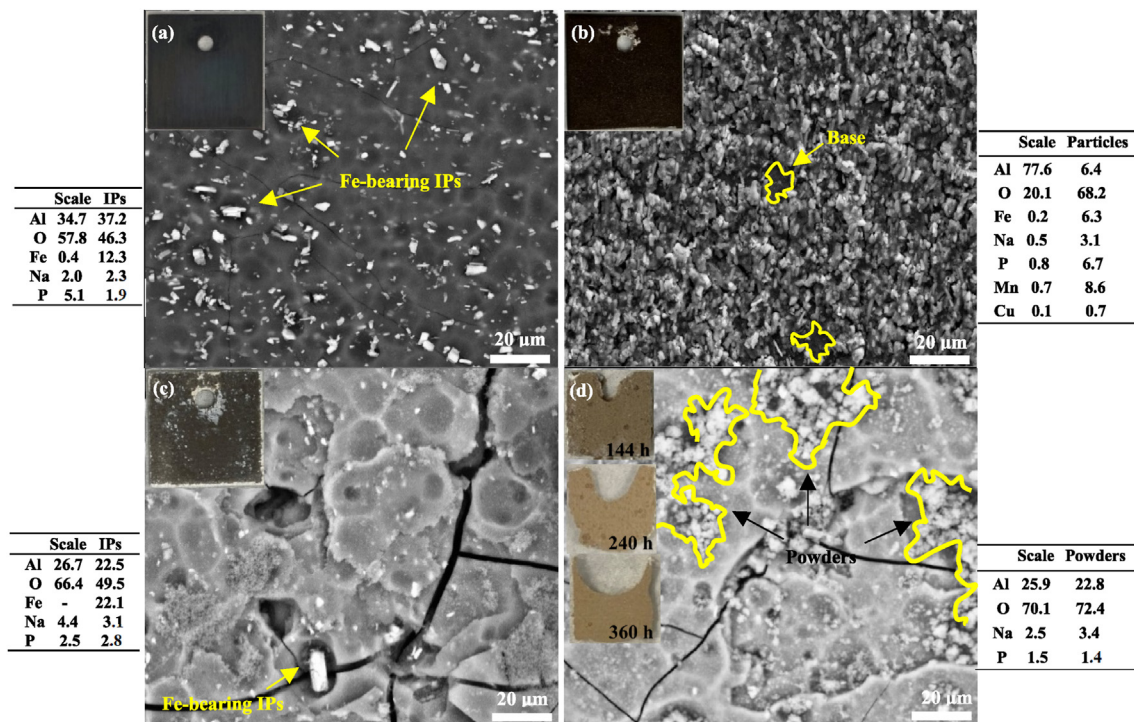


Fig. 5. SEM images of Al coupon in TSP-buffered solution with (a) pH 8.5 at 360 h; (b) pH 10.0 at 8 h; (c) pH 10.0 at 48 h; (d) pH 10.0 at 144 h, 240 h, 360 h.

dominates below 50 °C, bayerite below 90 °C, boehmite above 90 °C, and their solubility increased in the order of bayerite < boehmite < amorphous. More recent studies [38,39] showed that the oxide layer at 25 and 55 °C was gibbsite, and at 85 and 130 °C was primarily (pseudo-)boehmite in solution containing NaTB. The layers formed in TSP-buffered solution at 130 °C consisted of $\text{Al}(\text{OH})_3$ (gibbsite or bayerite) with a small fraction of AlPO_4 . This slight discrepancy between these literature data indicates the complexity of Al corrosion products, which could be affected by many factors, such as pH, temperature, time, flow velocity, specific ion adsorption, etc.

The morphology of coupon surfaces immersed in TSP-buffered solution with presence of insulations at pH 10.0 was also analyzed by the Optical Microscope (OM), as shown in Fig. 6a. A uniform greyish dull scale formed initially. Significant amounts of snow-flake-like particulates were attached on coupon surface. The particulates continued to form and fully cover the coupon surface after 360 h immersion, which indicates the occurrence of precipitation. The EDS analyses for the scale and powdery particulates show that the aluminum oxide is likely $\text{Al}(\text{OH})_3$ with slight of Si and Ca, which are constituents of both the fiberglass and the Ca-sil.

3.2. Solution with buffering NaTB

Fig. 7 displays the mass loss of coupons in NaTB-buffered solution. When there was no insulation, the coupon continued to dissolve and until completely dissolved in a few days. No scale formed on coupon surface. The data here were also fitted to the equation $[\text{ML}] = k \cdot t$, which provides a good approximation. The k in condition of pH 10.0 is around 47.88 mg/h, 2 times higher than that in condition of pH 9.5. The notable precipitation was found in these test solutions and the mass of sediments was presented in Fig. 7. More sediments were collected in the solution with higher pH. When insulations were present, the Al concentration reached equilibrium around 24 h. These results indicate that the insulation

could prohibit the Al corrosion by building a protective layer on it, and the high pH could exacerbate Al corrosion.

Fig. 8 shows SEM images of the coupon surface in solution with presence of insulations at pH 10.0. EDS analysis were performed on the visible residues at the edges of coupon (Fig. 8a) and flaky layer (Fig. 8b), the results suggest that the deposits are mainly the compound of Al and O. Shards of fiberglass were observed on the coupon surface after 360 h immersion (Fig. 8c). When insulations presented, the scale formed in TSP solution has a higher O concentration than that in NaTB solution, accordingly the scale here is presumed as a mixture of Al_2O_3 and $\text{Al}(\text{OH})_3$. While the powder formed in both solutions presents same chemical compositions. And the Fe-bearing IPs were only found at the beginning. The scale on the coupon surface is more likely of chemical origin, rather than being the result of particles settling on the surface because of the vertical orientation of the metal coupons in the bottle (with a small horizontal cross-sectional area).

4. Discussion and comparisons

Several studies have found that NaTB leads to a higher solubility of Al [16,29,18]. A comparison of time dependency of Al concentration is given in Fig. 9. The NaTB solution resulted in more Al release than TSP solution, although a higher pH in TSP solution. The Al concentration showed a steep rise in the first 24 h. After that, it tended to be steady in TSP solution. In comparison, a reduction tendency was observed in NaTB solution, suggesting that some dissolved aluminum precipitated from solution. However, these fine precipitates were not noticed under naked eyes and cannot be collected for analysis. The ICET program also suggested a high Al corrosion rate in NaTB solution when the pH above 8.0, while much lower when using TSP [40].

Matt [41] developed a model to describe the Al release kinetics as a function of pH, temperature and time. At $\text{pH} \geq 8$, release kinetics became nearly linear with time. Fig. 10 compares the mass

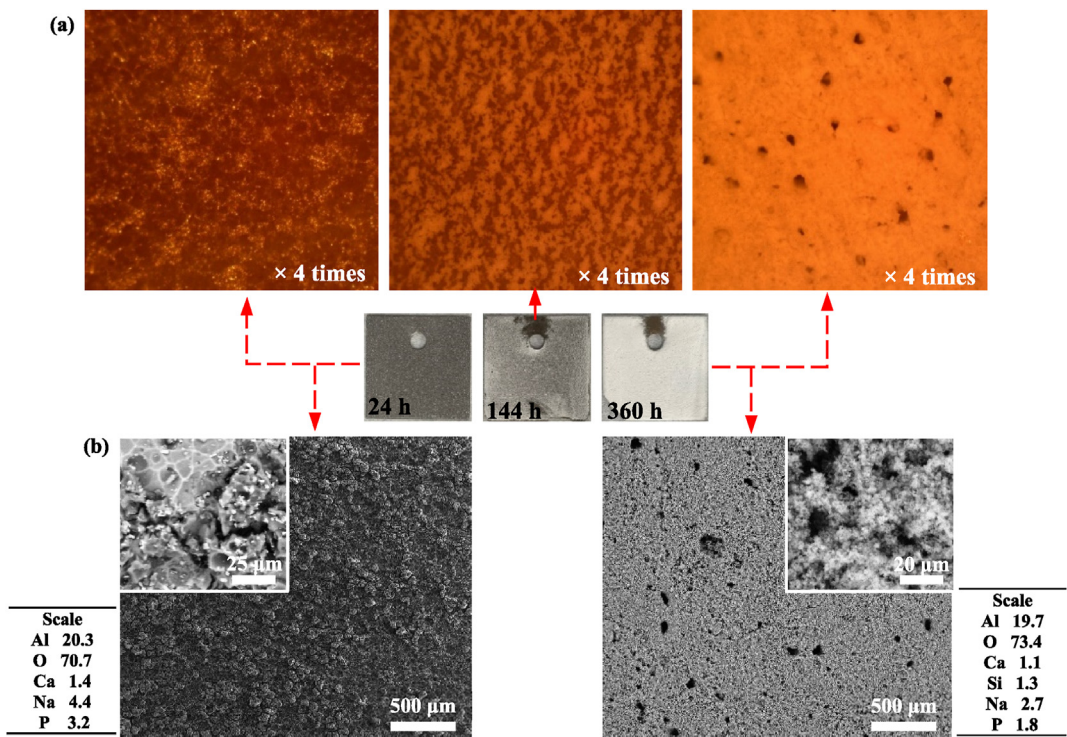


Fig. 6. Surface images of Al coupon in TSP solution at pH 10.0 with presence of insulation at 24 h, 144 h and 360 h (a) OM, (b) SEM.

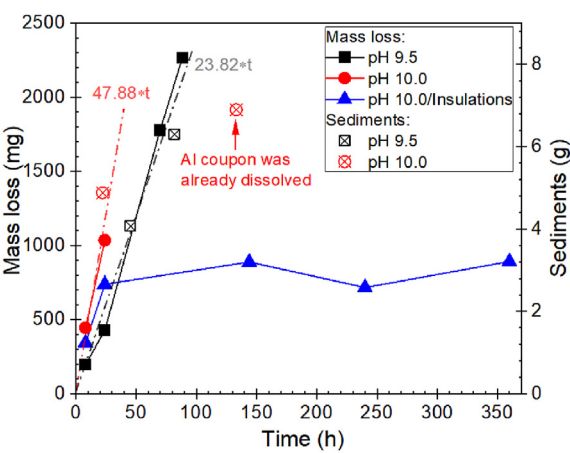


Fig. 7. Measured mass loss of coupon in NaTB-buffered solution and sediment weights.

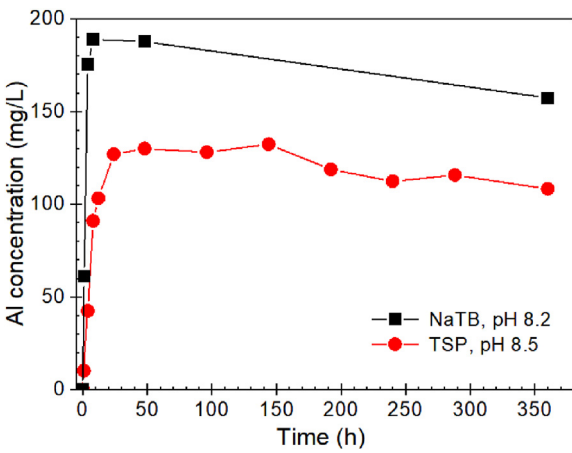


Fig. 9. Al concentration in less alkaline solution.

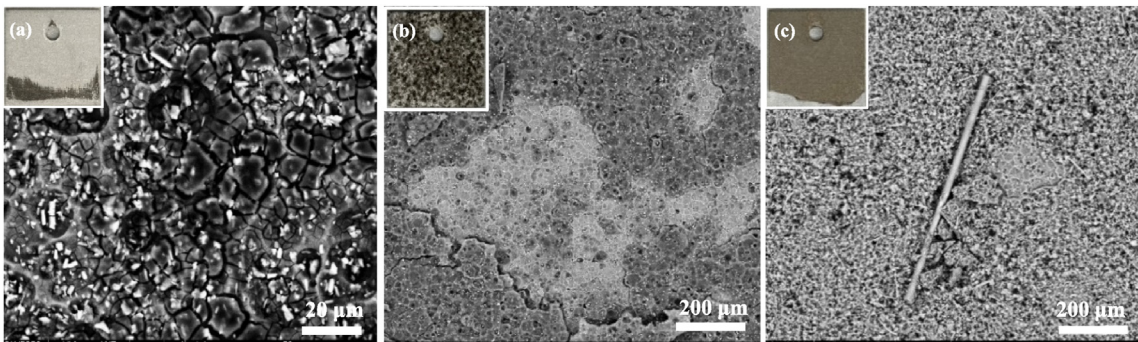


Fig. 8. SEM images of Al coupon in NaTB solution with presence of insulation at pH 10.0: (a)–(c) 8 h, 24 h and 360 h.

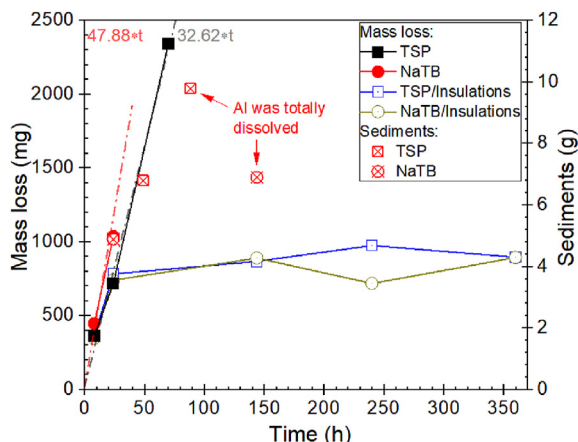


Fig. 10. A comparison of mass loss of coupons immersed in TSP/NaTB solutions and sediment weights.

loss of coupon in different solutions at pH 10.0. The coefficient k for coupon in NaTB solution is higher than that in TSP solution, showing that the Al dissolved more seriously in NaTB solution. In this study, the boron concentration in TSP and NaTB solution was similar, thus the P appears retarding the boron effect on Al release. Similar results were reported by Howe [42] that the presence of TSP could lead to a less corrosive environment for Al. However, more sediments were collected from TSP solution. Specially, the dissolution of each gram Al in TSP solution produced 3.63 g sediments, it is 2.53 g in NaTB solution. In the cases where insulations were present, there was a consistent tendency in mass loss between coupons immersed in TSP and NaTB solutions, which indicates the significant inhibition impact of Si on Al dissolution.

Corrosion products with different texture were found in bottles during tests. At the beginning, there was no significant precipitate and the solution was clear, while milky precipitates formed and settled down with solution cooling, difficult to filter and highly hydrated like gel, see Fig. 11. These precipitates were completely redissolved after solution was reheated to 85 °C. However, thermodynamically stable precipitates in TSP and NaTB solutions at 85 °C were observed as time processed (Fig. 12). And these precipitates could be easily extracted from solution and desiccated. Fig. 12b shows the less soluble precipitates formation process: from gray deposit at 48 h to brown and platelike deposit at 144 h. After cooling down the solution and removing the supernate, white deposits were observed in TSP solution (Fig. 12a), while no white precipitates formed in NaTB-buffered solution (Fig. 12c–e).

When the temperature of solution containing dissolved Al decreases with time, Al precipitation possibly occurs because the solution becomes supersaturated. The report NUREG/CR-6915 [43] showed that the crystallographic phase of Al hydroxide precipitates in alkaline solution depends on the degree of supersaturation. If the system was supersaturated with respect to a number of different

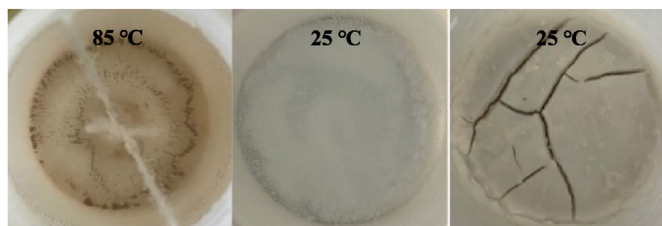


Fig. 11. Precipitates formed in solution with pH 10.0 at 24 h.

crystalline forms, the thermodynamically least stable form is quite often the first one to form, which is known as the “Ostwald Rule of Stages” [44]. Zhang et al. [45] reviewed the Al hydroxide solid phase formation in alkaline solution. They suggested that the Al hydroxide phase is dependent on pH, temperature, time, and uniformity of mixing reactants. And the precipitation sequence from supersaturated aluminate solutions is amorphous—pseudoboehmite—bayerite. Precipitation of Al hydroxide from the supersaturated state typically has an incubation time of less than an hour at 50 °C, while the phase transformation from amorphous or pseudoboehmite to thermodynamically more stable form (bayerite) occurs over a few weeks [46]. Our test found the less soluble precipitates in solution with pH 10.0 and 85 °C at 48 h, suggesting that the higher pH and temperature could enhance the transformation. Same texture of precipitates was also observed after 240 h and 360 h exposure (Fig. 12d and e). When the insulations were present, no insoluble precipitate was observed in solution at 85 °C. Less sediments precipitated after solution cooling. Adu-Wusu [47] studied the reaction of Si with gibbsite (stable crystalline $\text{Al}(\text{OH})_3$) in sodium aluminate solution. The study showed that adsorption of Si on gibbsite seed crystals reduces the gibbsite crystallization and increases the equilibrium solubility of gibbsite.

The test solutions with pH 10.0 were collected in a 15-ml tube for precipitation observation. The normalized precipitate volume is defined as the volume ratio of the precipitate region in solution to the total solution volume in the tube, as summarized in Fig. 13a. The precipitate volume in TSP solution is greater than that in NaTB solution under the same exposure time, consistent with the preceding finding that more sediments were collected from TSP solution (Fig. 10). These results indicate that the phosphate has potential to alter the solubility of Al hydroxide precipitates and produce more sediments. When the insulations were present, the precipitate volume reduced significantly. Chi [19] found that Si appears to act as a deflocculant for Al hydroxide precipitates and increases its solubility in borated high-purity water. The precipitation constantly occurred as solution cooling in most solutions. However, the precipitate volume declined steadily in NaTB solution without insulations from 24 to 96 h and precipitation ceased thereafter, suggesting that more crystalline precipitate formed from the solution. This hypothesis was confirmed by the ICP analysis that the Al concentration of the supernate solution samples at 144 h, 240 h and 360 h decreased continuously.

Two different types of precipitates were observed (Fig. 13b). After 1 h of stagnation, the sample of NaTB solution became cloudy and visible floccules formed and settled down readily, the precipitates were dense. In comparison, the sample of TSP solution presented as very fine suspension without settlement tendency. Left overnight, visible cotton-ball like coagulation was observed in TSP solution sample, but settled extremely slow, and slight gap among these loose clusters could be seen. Dense and snow-like precipitates were in the bottom of NaTB solution sample and the supernate solution became clear. Stanley [48] found that the collision rate between particle clusters and their sedimentation rate depends on the number of particles that constitute the individual clusters, or their size. The dense precipitates with high settling rate would more effectively cause the pressure drop across the fuel assembly [49]. Thus, the precipitates formed in NaTB buffering seem to raise more concerns regarding the chemical effects in GSI-191.

Bahn [21] conducted the long-term Al hydroxide precipitation tests and summarized Al hydroxide precipitation map in the ‘pH + p[Al]_T’ vs. temperature domain, as shown in Fig. 14. The ‘pH’ means the solution pH at the room temperature and ‘p[Al]_T’ denotes the negative log to the base 10 of the total Al content in solution either as dissolved or precipitated form in units of mol/kg.

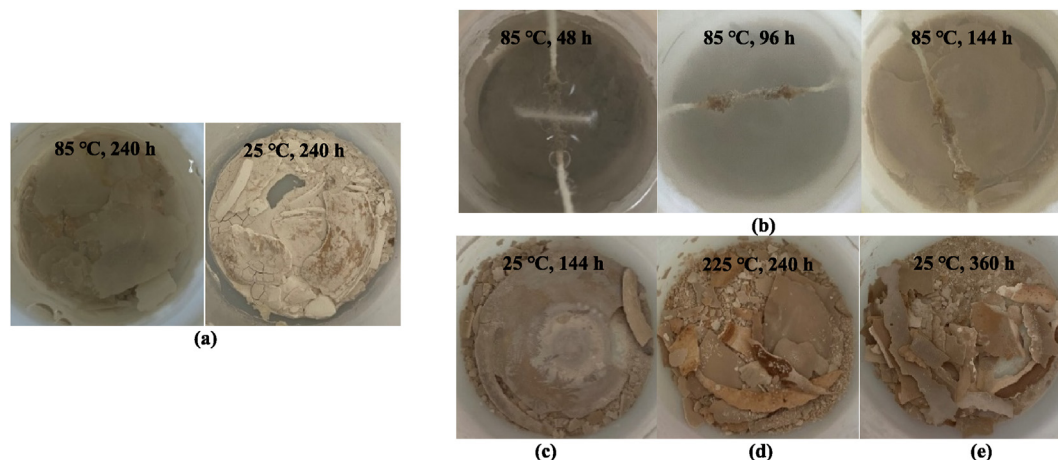


Fig. 12. Precipitates formed in solution of (a) TSP-pH 10.0 at 240 h; (b) NaTB-pH 10.0 from 48–144 h; (c–e) NaTB-pH 10.0 at 144 h, 240 h and 360 h.

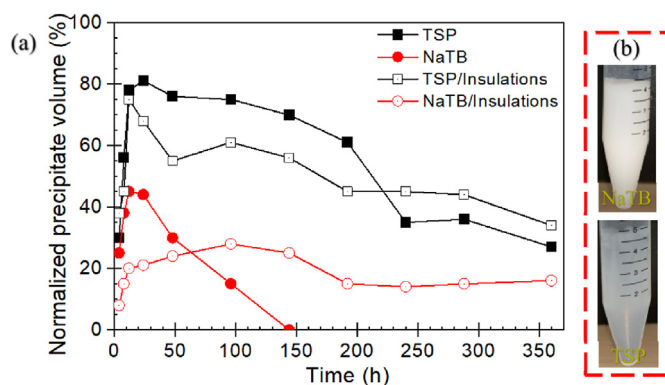


Fig. 13. Precipitates in solution samples (a) normalized precipitate volume at different time, (b) images of precipitates.

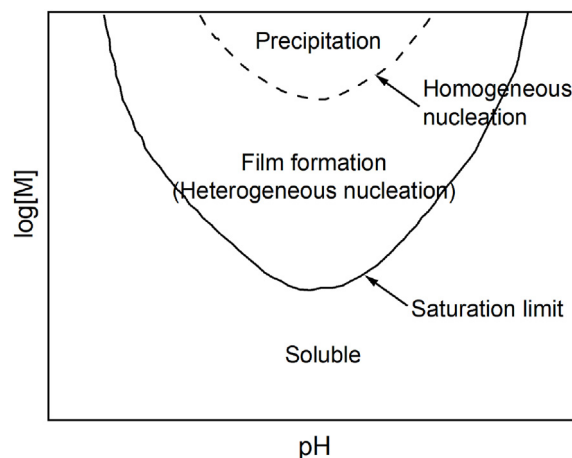


Fig. 15. Schematic solubility diagram for species in water.

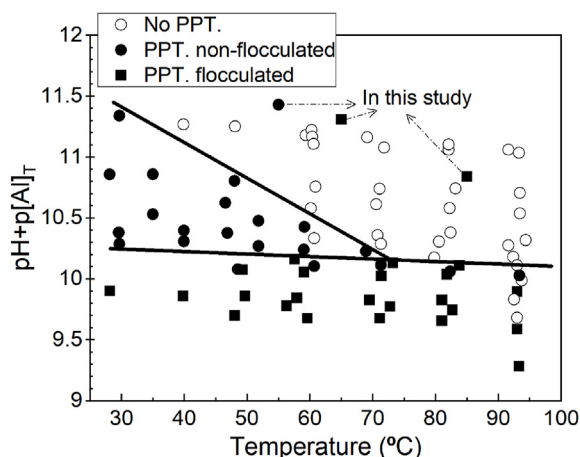


Fig. 14. Al hydroxide precipitation map in the 'pH + p[Al]_T' vs. temperature domain based on literature data.

Three distinct regions were revealed: no precipitation region (open circle symbol), non-flocculated precipitation region (solid circle symbol), and flocculated precipitation region (solid square symbol). It should be noted that since precipitation/non-precipitation was determined by visual observation, extremely fine precipitates (<100 nm) might be present in non-precipitation region. However,

three data points obtained from our tests are located above the proposed boundary line. Fig. 15 shows the schematic solubility diagram for chemical species in water. Above the saturation limit line, the solution becomes supersaturated. However, the degree of supersaturation is not enough to induce homogeneous nucleation. Instead, heterogeneous nucleation on any given surface could happen. If interactions between the growing nucleus and a substrate surface represent a lower net interfacial energy than the particle-solution interfacial energy, heterogeneous nucleation is preferred over homogeneous nucleation [50]. The three data points obtained from this study, shown in Fig. 14, can be explained by the possibility of heterogeneous nucleation. IPs may provide extra surface so that heterogeneous nucleation of Al hydroxide occurs on the IP surface at the condition where homogeneous nucleation cannot occur due to low supersaturation. This assumption was also confirmed by notable higher O concentration in IPs compared with substrate. Thus, it is conjectured that IPs observed in coupon surfaces act as seeds readily induce precipitation by providing surface area for heterogeneous Al hydroxide precipitation.

The XRD spectra of precipitates from test TSP/pH 10.0 at 360 h and test NaTB/pH 10.0 at 144 h and 240 h reveals that the precipitates are boehmite (γ -AlOOH), as shown in Fig. 16a. The precipitates formed at solution with insulations were mainly mixture of sodium tetraborate hydrate and boehmite, as shown in Fig. 16b.

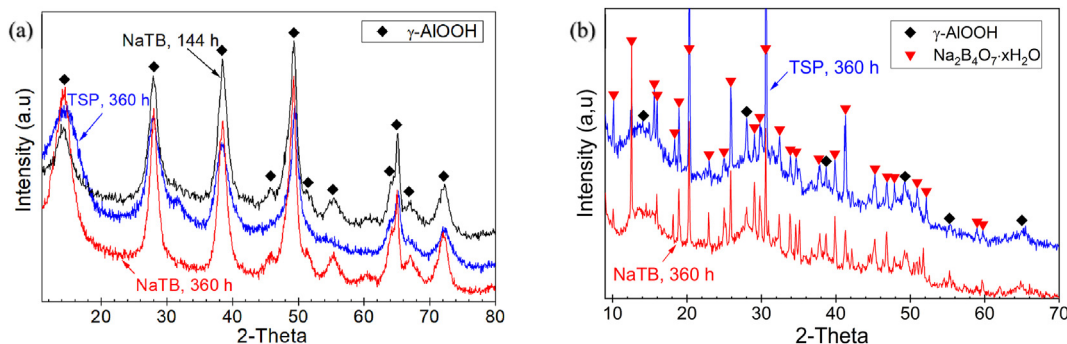


Fig. 16. XRD spectrum for precipitates formed in TSP/NaTB solution at pH 10.0 (a) without insulations, (b) with insulations.

However, the measured peaks do not precisely match the albite ($\text{NaAlSi}_3\text{O}_8$) or analcime ($\text{NaAlSi}_2\text{O}_6 \cdot \text{H}_2\text{O}$), so it is difficult to confirm whether the observed peaks are from sodium aluminosilicate or some other phase, although a slight of silicon was detected by EDS. Thus, uncertainties make it difficult to determine whether sodium aluminosilicate phase formed in solution with exposed insulations, and further examination would be necessary to obtain more conclusive results.

5. Conclusions

This study simulated a variety of chemical environments in containment pool after LOCA and monitored the chemical system for 15 days to identify the presence, composition and physical characteristics of chemical products generated from Al corrosion.

The intense dissolution of aluminum in more-caustic solution ($\text{pH} \geq 9.5$) raises the concern that the local area with high pH in containment pool could threaten integrity of aluminum materials and form significant precipitates. The upper limit of pH control for containment pool after LOCA could reach 8.5 because a protective layer readily formed at pH 8.5 in this study. The use of NaTB buffering should be considered to be limited in pH control after LOCA, because the Al was more corroded in NaTB buffering, and the precipitates formed in NaTB solution more likely cause severe blockage and head loss in fuel assemblies. No solid proof indicates the formation of $\text{NaAlSi}_3\text{O}_8$ in solution containing 2 g/L of insulations. Comparing with the $\text{NaAlSi}_3\text{O}_8$, the AlOOH should raise more concerns in GSI-191. The IPs originating from alloy could act as seeds by providing extra surface area for heterogeneous Al hydroxide precipitation. The high temperature and pH can enhance the transformation of Al precipitates to a stable crystalline form. The scales formed under the condition that insulations were present was the most efficient one to restrain Al corrosion and the Si appears to act as a deflocculation that prohibit Al hydroxide precipitating, it provides a potential idea on anticorrosion method design. Although this study provides some information for GSI-191, the effects of pH, temperature and ions on Al corrosion and the corresponding mechanisms were not thoroughly investigated. Further in-depth investigation is necessary to perform.

Declaration of competing interest

The authors declare that they have no known competing financial interests or personal relationships that could have appeared to influence the work reported in this paper.

Acknowledgements

The first author (Da Wang) would like to acknowledge the

NCEPU Scholarship Fund and Dr. Fenglei Niu who is the doctoral supervisor of Da Wang at NCEPU for his care and encouragement. All the research was conducted at Virginia Tech and was supported by the corresponding author's (Jinsuo Zhang) Startup funds.

References

- [1] NRC, NUREG/CR-6988, Evaluation of Chemical Effects Phenomena in Post-LOCA Coolant, Nuclear Regulatory Commission, Washington, DC, 2008.
- [2] USNRC, Potential for Degradation of the ECCS and the Containment Spray System after a LOCA Because of Construction and Protective Coating Deficiencies and Foreign Material in Containment, Nuclear Regulatory Commission, 1998.
- [3] NRC, Potential Impact of Debris Blockage on Emergency Recirculation during Design Basis Accidents at Pressurized Water Reactors, Nuclear Regulatory Commission, Washington DC, 2004.
- [4] R.C. Johns, B.C. Letellier, K.J. Howe, A.K. Ghosh, Small-scale Experiments: Effects of Chemical Reactions on Debris-Bed Head Loss, Nuclear Regulatory Commission, 2003.
- [5] A.K. Ghosh, K.J. Howe, A.K. Maji, B.C. Letellier, R.C. Jones, Head loss characteristics of a fibrous bed in a PWR chemical environment, Nuclear Technology 157 (2007) 196–207.
- [6] J. Dallman, B. Letellier, J. Garcia, J. Madrid, W. Roesch, D. Chen, K. Howe, L. Archuleta, F. Sciacca, B.P. Jain, Integrated Chemical Effects Test Project: Consoli-Dated Data Report, Nuclear Regulatory Commission, 2016.
- [7] C.B. Bahn, Chemical effects on PWR sump strainer blockage after a loss-of-coolant accident: review on U.S. Research efforts, Nuclear Engineering and Technology 45 (2013) 295–310.
- [8] D. Wang, F.L. Niu, R.X. Liang, et al., Assessment of head loss through LOCA generated debris deposited in PWR fuel assemblies, Annals of Nuclear Energy 137 (2020), 107037.
- [9] J.K. Suh, J.W. Kim, S.G. Kwon, et al., Experimental study of pressure drops through LOCA-generated debris deposited on a fuel assembly, Nuclear Engineering and Design 289 (2015) 49–59.
- [10] J.W. Evancho, J.T. STALEY, Kinetics of precipitation in aluminum alloys during continuous cooling, Metallurgical Transactions 43 (1974).
- [11] Y.J. Choi, S.W. Lee, H.T. Kin, Preliminary Evaluation of Long-Term Cooling Considering Chemical Precipitation and Subsequent Impact on the Recirculating Fluid, Jeju, Korea, 2010.
- [12] J.C. Griess, A.L. Bacarella, Design Considerations of Reactor Containment Spray Systems – Part III. The Corrosion of Materials in Spray Solutions, Oak Ridge National Laboratory, Tennessee, 1969.
- [13] J. Piippo, T. Laitinen, P. Sirkka, Corrosion Behavior of Zinc and Aluminum Simulated Nuclear Accident Environments, Finnish Center for Radiation and Nuclear Safety, Helsinki, Finland, 1997.
- [14] V. Jain, X. He, Y.M. Pan, Corrosion Rate Measurements and Chemical Speciation of Corrosion Products Using Thermodynamic Modeling of Debris Components to Support GSI-191, Center for Nuclear Waste Regulatory Analyses, San Antonio, TX, 2005.
- [15] D. Chen, K.J. Howe, J. Dallman, B.C. Letellier, Experimental analysis of the aqueous chemical environment following a loss-of-coolant accident, Nuclear Engineering and Design 237 (2007) 2126–2136.
- [16] J.H. Park, K. Kasza, B. Fisher, J. Oras, K. Natesan, W.J. Shack, NUREG/CR-6913: Chemical Effects Head-Loss Research in Support of Generic Safety Issue 191, Nuclear Regulatory Commission, 2006.
- [17] A.E. Lane, T.S. Andreychev, W.A. Byers, E.J. Lahoda, R.D. Reid, WCAP-16530-NP-A: Evaluation of Post-accident Chemical Effects in Containment Sump Fluids to Support GSI-191, Westinghouse, 2008.
- [18] C.B. Bahn, K.E. Kasza, W.J. Shack, K. Natesan, Technical Letter Report on Evaluation of Chemical Effects: Studies on Precipitates Used in Strainer Head Loss Testing, Nuclear Regulatory Commission, 2008.
- [19] C.B. Bahn, K.E. Kasza, W.J. Shack, K. Natesan, P. Klein, Evaluation of precipitates

- used in strainer head loss testing. Part I. Chemically generated precipitates, *Nuclear Engineering and Design* 239 (2009) 2981–2991.
- [20] C.B. Bahn, K.E. Kasza, W.J. Shack, K. Natesan, P. Klein, Evaluation of precipitates used in strainer head loss testing Part II. Precipitates by in situ aluminum alloy corrosion, *Nuclear Engineering and Design* 241 (2011) 1926–1936.
- [21] C.B. Bahn, K.E. Kasza, W.J. Shack, K. Natesan, P. Klein, Evaluation of precipitates used in strainer head loss testing Part III Long-term aluminum hydroxide precipitation tests in borated water, *Nuclear Engineering and Design* 241 (2011) 1914–1925.
- [22] S.J. Kim, K. Howe, CHLE-019 Test Results for Chemical Effects Tests Stimulating Corrosion and Precipitation (T3 & T4), University of New Mexico, Albuquerque, NM, 2013.
- [23] S.J. Kim, CHLE-020: Test Results for a 10-day Chemical Effects Test Simulating LBLOCA Conditions (T5), University of New Mexico, Albuquerque, NM, 2014.
- [24] B.N. Bachra, O.R. Trautz, S.L. Simon, Precipitation of calcium carbonates and phosphates—III: the effect of magnesium and fluoride ions on the spontaneous precipitation of calcium carbonates and phosphates, *Archives of Oral Biology* 10 (1965) 731–738.
- [25] S.S. Olson, Investigation of Calcium Orthophosphates in a Post-LOCA Nuclear Reactor Containment, University of New Mexico, Albuquerque, New Mexico, 2015.
- [26] S.J. Kim, J. Leavitt, K. Hammond, L. Mitchell, E. Kee, F.K. Howe, Experimental study of chemical effects on ECCS strainer head loss and flow sweep test with two debris beds (blender-processed debris bed vs. NEI-processed debris bed), in: *Proceeding of American Nuclear Society Winter Conference*, 2013.
- [27] S.S. Olson, A. Ali, CHLE-SNC-013: 4000 Series: Calcium Summary Report. Rev.3, University of New Mexico, Albuquerque, NM, 2015.
- [28] ASTM, Standard Practice for Preparing, Cleaning, and Evaluating Corrosion Test Specimens, ASTM G1-03, 2017.
- [29] R.D. Reid, K.R. Crytzer, A.E. Lane, WCAP-16785-NP: Evaluation of Additional Inputs to the WCAP-16530-NP Chemical Model, Westinghouse Electric Company Pittsburgh, PA, 2007.
- [30] S. Guo, J. J. Leavitt, X. Zhou, Y. Xie, S. Tietze, Y. Zhu, A. Lawver, E. Lahti, J. Zhang, Effects of flow, Si inhibition, and concurrent corrosion of dissimilar metals on the corrosion of aluminium in the environment following a loss-of-coolant, *Corrosion Science* 128 (2017) 100–109.
- [31] N. Birbilis, R.G. Buchheit, Electrochemical characteristics of intermetallic phases in aluminum alloys: an experimental survey and discussion, *Journal of the Electrochemical Society* 152 (2005) B140–B151.
- [32] O. Seri, K. Furumata, Effect of Al–Fe–Si intermetallic compound phases on initiation and propagation of pitting attacks for aluminum 1100, *Materials and Corrosion* 53 (2002) 111–120.
- [33] A. Kosari, F. Tichelaar, P. Visser, H. Zandbergen, H. Terrynd, J.M.C. Mol, Dealloying-driven local corrosion by intermetallic constituent particles and dispersoids in aerospace aluminium alloys, *Corrosion Science* 177 (2020), 108947.
- [34] J. Huang, D. Lister, S. Uchida, L. Liu, The corrosion of aluminium alloy and release of intermetallic particles in nuclear reactor emergency core coolant: implications for clogging of sump strainers, *Nuclear Engineering and Technology* 51 (2019) 1345–1354.
- [35] D. LaBrier, A. Ali, K.J. Howe, E.D. Blandford, Integrated chemical effects head loss experiments using multiconstituent fibrous debris beds, *Journal of Nuclear Engineering and Radiation Science* 3 (2017), 011006-1–011006-14.
- [36] H. Godard, *The Corrosion of Light Metals*, Wiley, New York, 1967.
- [37] C. Vargel, *Corrosion of Aluminum*, Elsevier, New York, 2004.
- [38] Y. Xie, A. Leong, J. Zhang, J.J. Leavitt, Aluminum alloy corrosion in boron-containing alkaline solutions, *Materials and Corrosion* 70 (2019) 810–819.
- [39] S. Guo, B. Dsouza, Y. Xie, A. Leong, J.J. Leavitt, J. Zhang, Aluminum corrosion in reactor containment environment following a loss of coolant accident (LOCA): high-temperature flow loop tests, *Corrosion Science* 151 (2019) 122–131.
- [40] D. Chen, K.J. Howe, J. Dallman, B.C. Letellier, Corrosion of aluminum in the aqueous chemical environment of a loss-of-coolant accident at a nuclear powerplant, *Corrosion Science* 50 (2008) 1046–1057.
- [41] M. Edwards, J. Semmler, D. Guzonas, H.Q. Chen, A. Toor, Aluminum corrosion product release kinetics, *Nuclear Engineering and Design* 288 (2015) 163–174.
- [42] K. Howe, L. Mitchell, S.J. Kim, E. Blandford, E. Kee, Corrosion and solubility in a TSP-buffered chemical environment following a loss of coolant accident: part 1—aluminum, *Nuclear Engineering and Design* 292 (2015) 296–305.
- [43] M. Klasky, J. Zhang, M. Ding, B. Letellier, Aluminum Chemistry in a Prototypical Post-loss-of-a-coolant-accident, Pressurized-Water-Reactor Containment Environment, Nuclear Regulatory Commission, 2006.
- [44] H.A. van Straten, B.T. W. Holtkamp, P.L. de Bruyn, Precipitation from supersaturated aluminate solutions: I. Nucleation and growth of solid phases at room temperature, *Journal of Colloid and Interface Science* 98 (1984) 342–362.
- [45] J. Zhang, M. Klasky, B.C. Letellier, The aluminum chemistry and corrosion in alkaline solutions, *Journal of Nuclear Materials* 384 (2009) 175–189.
- [46] H.A. van Straten, P.L. de Bruyn, Precipitation from supersaturated aluminate solutions: II. Role of temperature, *Journal of Colloid and Interface Science* 102 (1984) 260–277.
- [47] K. Adu-Wusu, W.R. Wilcox, Kinetics of silicate reaction with gibbsite, *Journal of Colloid and Interface Science* 143 (1991) 127–138.
- [48] S.B. Grant, J.H. Kim, C. Poor, Kinetic theories for the coagulation and sedimentation of particles, *Journal of Colloid and Interface Science* 238 (2001) 238–250.
- [49] D. Wang, B.C. Chang, T.Y. Zhang, S.C. Tan, F.L. Niu, Evaluation of chemical effects on fuel assembly blockage following a loss of coolant accident in nuclear power plants, *International Journal of Energy Research* 44 (2020) 5488–5499.
- [50] C.B. Bahn, K.E. Kasza, W.J. Shack, K. Natesan, Technical Letter Report on Evaluation of Head Loss by products of Aluminum Alloy Corrosion, Argonne National Laboratory, Argonne, 2008.